

# A Dynamic Constraint-based Modelling (DCBM) Approach With Alternative Metabolic Objective Functions Predicts The impact of Oxidative Stress on Stored Red Blood Cells (RBCs)

Mohammadreza Yasemi\* Michel Prudent<sup>\*\*,\*\*\*,\*\*\*\*</sup>  
Mario Jolicoeur\*

\* *Research Laboratory in Applied Metabolic Engineering, Department of Chemical Engineering, École Polytechnique de Montréal, P.O. Box 6079, Centreville Station, Montréal (Québec), H3C 3A7 Canada. (e-mail: mohammadreza.yasemi@polymtl.ca, mario.jolicoeur@polymtl.ca)*

\*\* *Laboratoire de Recherche sur les Produits Sanguins, Transfusion Interrégionale CRS, Epalinges, Switzerland. (e-mail: michel.prudent@itransfusion.ch)*

\*\*\* *Centre de transfusion sanguine, Faculté de Biologie et Médecine, Université de Lausanne, Lausanne, Switzerland*

\*\*\*\* *Center for Research and Innovation in Clinical Pharmaceutical Sciences, Lausanne University Hospital and University of Lausanne, Lausanne, Switzerland*

**Abstract:** Mathematical metabolic modelling is a systematic endeavour to allow identifying the main causes of an observed metabolic change and to estimate the consequences of an imposed metabolic perturbation regarding a biosystem. Dynamic Constraint-based modelling (DCBM) has delivered promising results in metabolic engineering and in bioprocess design by providing mechanistically relevant systems-level knowledge of a network of bioreactions. Here, we seek to establish a DCBM approach that leverages convex optimization and nonlinear regression mathematical toolkit to estimate dynamic intracellular metabolic flux distributions in stored Red Blood Cells (RBCs) for transfusion purposes. First, we developed an *ad-hoc* metabolic network including 77 reactions and 74 metabolites, second, we adapted Flux Variability Analysis (FVA) technique to quantify the connection between exometabolomic dynamics and the dynamics of feasible intracellular reaction flux ranges. We have obtained fine-grained flux range dynamics of the intracellular reactions for the benchmark data published in (Bordbar et al., 2016). Then, we defined four objective functions regarding the accumulation of oxidative stress in stored RBCs for performing a dynamic Flux Balance Analysis (DFBA). In all four cases, time-resolved flux predictions were obtained respecting the imposed equality and inequality constraints. Last, we adapted a quadratic programming (QP) approach to calculate the Euclidean distance between the dynamic optimum flux vectors. The DCBM approach we have developed herein along with the developed metabolic network showed being suitable for the computational analysis of RBCs metabolic behaviour, and it is thought to be useful for other biosystems.

Copyright © 2022 The Authors. This is an open access article under the CC BY-NC-ND license (<https://creativecommons.org/licenses/by-nc-nd/4.0/>)

**Keywords:** Mathematical Programming, Biological Systems Modelling, Metabolic Network Modelling, Constraint-based Modelling, Linear Programming Problem, Oxidative Stress, Red Blood Cells

## 1. INTRODUCTION

The integration of metabolomics data into mechanistic models can provide a practical understanding of a metabolic network at the system level. Guiding model construction and validation, the availability of experimental data allows elucidating mechanisms behind an observed metabolic change. Thus, mathematical modelling enables researchers to estimate consequences of an imposed metabolic perturbation in several research interests such as looking at metabolic energy states, bioproduction optimization, computational strain design and drug development (Lakrisenko and Weindl, 2021; Laflaquiere et al., 2018). The current state of metabolic modelling approaches and computational systems biology methods have been reviewed recently (Yasemi and Jolicoeur, 2021; Volkova et al., 2020). In this work, we have selected quiescent non-growing stored Red Blood Cells (RBCs) as the biosystem under study, integrating metabolomics data to study the accumulation of storage lesions in stored RBCs (Paglia et al., 2016; Roback et al., 2014; Bardyn et al., 2020, 2017a; Bordbar et al., 2011). In transfusion medicine, the storage lesions may have detrimental health consequences for the patients transfused with old stored RBC concentrates (Bardyn et al., 2017b; Yoshida et al., 2019). Here, we developed an *in-silico* workflow for investigating the dynamics of the enzymatic and non-enzymatic oxidative stress defence mechanisms in RBC storage conditions.

In this study, we present a dynamic constraint-based modelling (CBM) workflow that integrates the extracellular time series data of stored RBC for an *ad-hoc* metabolic network of RBC. The goal is to predict the unknown intracellular fluxes, from a combination of measured transport fluxes, without any *a priori* assumptions regarding potential metabolic shifts in the metabolic network magnitude and direction during the RBC storage time.

## 2. STOICHIOMETRIC MODEL RECONSTRUCTION AND PARTITIONING

The stoichiometric model of the RBC metabolic network was reconstructed iteratively from the physiological knowledge on RBCs and the previously published genome-wide metabolic model for this biological system (Bordbar et al., 2011). The stoichiometric matrix was partitioned based on a distinction between the intra- and extracellular spaces as given in equation (2),

$$\begin{aligned} \frac{\Delta M_{int}}{\Delta t} &= S.v \\ &= [S_{II} \ S_{IT}] \begin{bmatrix} v_{Intra} \\ v_{Transport} \end{bmatrix} = b_m, \end{aligned} \quad (1)$$

$$lb \leq v \leq ub \quad (2)$$

where the vector  $\Delta M_{int}$  is a vector of dimension  $m$  of intracellular metabolites change, the vector  $v$  represents reaction fluxes with dimension  $n$ , which stands for the collective set of  $v_{Intra}$  and  $v_{Transport}$ . The stoichiometric matrix  $S$  of dimension  $m \times n$  is divided into  $S_{II}$  representing the stoichiometric relation of intracellular metabolites

to the intracellular reactions and  $S_{IT}$ , which represents the relationship between the metabolites passing the system boundary and transport reactions. The vector  $b_m$  is non-zero right-hand side of the equation,  $lb_n$  and  $ub_n$  are the lower and upper bounds of the flux vector, respectively. We adapted the pseudo steady state assumption if  $\Delta t \ll$  sample intervals with  $t$  being a continuous time vector. Thus, in equation (2) we consider  $b_m = 0$  (Segel and Slemrod, 1989).

In the iterative procedure of the metabolic network reconstruction, we modified the metabolites by lumping and distributing, and we modified the reactions by adding (or removing) transport and sink reactions followed by explanatory simulations. The final version of our stoichiometric model describing the metabolic network was used throughout the next sections (table 1).

## 3. NONLINEAR FITTING OF THE EXOMETABOLOMICS

To avoid model infeasibility due to the inaccuracies emerging from noisy experimental measurements, we run a nonlinear regression data-fit for each of the twelve measured extracellular metabolites. A set of independent exponential continuous functions is fitted to the extracellular metabolites concentration curves as described in equation (3).

$$M_{ext}^{sim}(p, t) = p_1 * \exp(p_2 * t) \quad (3)$$

where  $p$  is the vector of parameters to be estimated, and  $M_{ext}^{sim}$  represents the simulation values of extracellular metabolites as a function of the continuous time vector  $t$ . The parameter estimation formulation and the nonlinear objective function are given in equation (4).

$$\min_{p \in \mathbb{R}^2} f(p) := \sum_{k=1}^N \left( M_{ext}(t_k) - M_{ext}^{sim}(p, t_k) \right)^2 \quad (4)$$

Such that  $t_1 = 0$ ,  $t_N = 42$ ,  $k \in \{1, 2, \dots, N\}$   
 $N = 14$

$M_{ext}(t_k)$  represents the experimental value of an extracellular metabolite at time point  $t_k$  (in days), where  $k$  is the number of experimental data acquisition ending at day 42 after a total of  $N = 14$  observations (see (Bordbar et al., 2016) for detailed explanation of the experimental setup). Then, the 95% confidence interval of the estimated parameters is determined by *nlparci* function in MATLAB using the Jacobian of the nonlinear fit function. We used the derivative of the smooth fit functions to calculate instantaneous transport fluxes. Noteworthy, the derivatives were calculated at the lower and upper bounds of the estimated parameters, as well as at the estimated parameter values (Fig. 1). As such, we accounted for uncertainty in the measurements and determined transport flux bounds in section 5. The derivatives were calculated as in equation (5).

$$\frac{\partial M_{ext}^{sim}(p, t)}{\partial t} = p_1 * p_2 * \exp(p_2 * t) \quad (5)$$

Table 1. The RBC metabolic model configuration

Model component	Total Number	# Intracellular	# Transport or Extracellular (measured)	# Sink	# Blocked or Dead end
Reactions	77	53	16 (12)	8	0
Metabolites	74	57	17 (12)	N/A	0

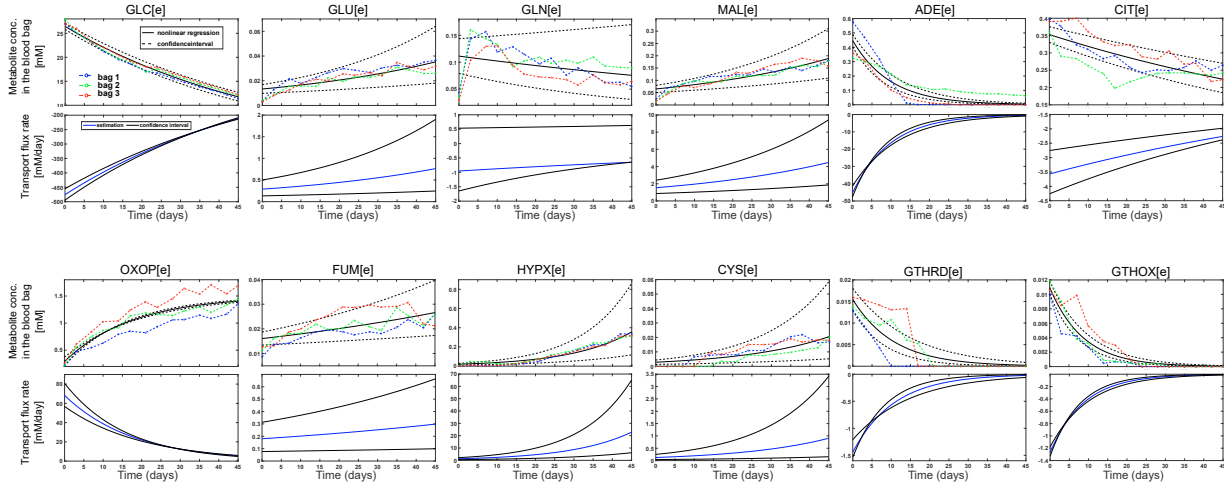


Fig. 1. **Nonlinear regression fit of the blood bag ingredients concentration values and the associated transport flux rates** The exponential regression fit curves (solid black lines) with 95% confidence interval of the estimated parameters (dashed black lines). The lower and upper bounds of the twelve transport flux rates are assigned based on this panel. The bag numbers and experimental values (circles) for  $N = 14$  experimental time points are taken from the second supplementary document of (Bordbar et al., 2016).

#### 4. DEFINING SIMULATION TIME

We define a separate time vector  $tsim$  to use in the following sections, this is the time vector on which our constraint-based modelling method goes forward in time until ending at  $tsim_L = t_N = 42$  (days).

$$\begin{aligned}
 t_1 \leq tsim_q \leq t_N \\
 \text{Such that } q \in \{1, 2, \dots, L\} \\
 L = 45
 \end{aligned} \quad (6)$$

where  $L$  represents the number of simulation points. In this study, we defined this number equal to 45 in a trade-off between model feasibility and the predefined computational cost limit. Moreover, the simulation time points are linearly distributed and each interval is roughly equal to one day in the experimental context.

#### 5. DYNAMIC FLUX VARIABILITY ANALYSIS (DFVA) TO IDENTIFY THE ALLOWABLE INTRACELLULAR FLUX RANGES

We ran FVA at each of the simulation time points to identify the intracellular flux bounds based on the solution of  $2n$  number of Linear Programming (LP) problems optimizing for min/max of each reaction flux. The advantage of calculating intracellular flux ranges by this method is that the estimated ranges are unbiased with respect to any assumed objective function for the cell functioning during the storage time. However, for the calculated ranges to be surrounded by default flux bounds, i.e., not to be redundant, iterative modification of the metabolic network structure was required. The ranges

identified by DFVA were narrower than the default  $-1000$  to  $1000$  ( $mmol.L^{-1}.day^{-1}$ ) range for 83% of the intracellular fluxes.

$$\begin{aligned}
 \min / \max f(\mathbf{v}) &:= v_i \quad v_i \in \begin{bmatrix} \mathbf{v}_{Intra} \\ \mathbf{v}_{Transport} \end{bmatrix} \\
 \text{Subject to} & \quad S \cdot \mathbf{v} = 0; \\
 lb_j \leq & \quad v_j \leq ub_j, v_j \in \mathbf{v}_{Transport}
 \end{aligned} \quad (7)$$

where  $lb_j$  and  $ub_j$  values were calculated in section 3.

#### 6. DYNAMIC FLUX BALANCE ANALYSIS (DFBA) BASED ON SEVERAL THEORETICAL OBJECTIVES

First, we constrained a sub-set of the transport fluxes  $\mathbf{v}_{Transport}$  including twelve fluxes as shown in Fig. 1. The selected measured consumption/secretion rates constituted 75% and 21% of transport and intracellular fluxes, respectively (table 1). Then, we defined four different objective functions and studied the solutions (see Results and Discussion). The objective functions were set to the following  $f_i(\mathbf{v})$ 's (reactions are given in Fig. 3).

- (1) Set 1: Limited glucose ( $-v1$ ).
- (2) Set 2: Maximal ROS tolerance ( $v53$ ).
- (3) Set 3: Minimal ROS tolerance ( $-v53$ ).
- (4) Set 4: Maximal Oxidative PPP (Ox-PPP) activity ( $v14$ ).

We considered Set 1 the nominal scenario, Set 2 the ideal antioxidant scenario within the experimental constraints, Set 3 the worst case scenario, and Set 4 as a relevant metabolic scenario of interest. Thus, the LP problem in

equation (8) was solved regarding each set at consecutive simulation time points.

$$\begin{aligned} \min_{\mathbf{v} \in \mathbb{R}^n} f_i(\mathbf{v}) &:= \mathbf{c}_i^T \mathbf{v} & i = 1, 2, 3, 4 \\ \text{Subject to } S \cdot \mathbf{v} &= 0; \\ lb_i &\leq v_i \leq ub_i, v_i \in \mathbf{v}_{Intra} \\ lb_j &\leq v_j \leq ub_j, v_j \in \mathbf{v}_{Transport} \end{aligned} \quad (8)$$

where  $(lb_i, ub_i)$  and  $(lb_j, ub_j)$  values were calculated in equations (7) and (5), respectively.

## 7. RESULTS AND DISCUSSION

### 7.1 Development of an ad-hoc metabolic network

The metabolic network was reconstructed for explaining RBCs oxidative metabolism, the model scope involves cofactor-dependent enzymes participating in Reactive Oxygen Species (ROS) termination bioreactions, and glutathione metabolism as our central modelling objective. Moreover, the major pathways dominating intracellular metabolism of RBCs were accounted for as shown in Fig. 3. To validate the developed metabolic network, we optimized the nominal objective function (Set 1) at the  $N$  consecutive experimental time points ( $N = 14$ ) reported in (Bordbar et al., 2016) for RBCs that were suspended in 100 mL of SAGM (Saline, Adenine, Glucose, Mannitol) additive solution. At first, the reconstruction needed several rounds of modifications to find dynamic feasible solutions. However, when the feasible solutions appeared for the first time, i.e., the metabolic network was validated, the extracted stoichiometric model supported DFBA simulations for  $L = 45$  simulation time points regarding the four objectives with only minor modifications (Fig. 2).

### 7.2 Linking the transport flux rates to unbiased intracellular flux ranges

The developed extension of CBM for describing time-resolved dynamics of the RBC internal metabolic network starts off from the nonlinear exometabolomics fitting (section 3), which converts the discrete measurements into differentiable analytical functions. However, it is noteworthy that neither the exponential analytical functions nor the estimated independent parameters in equation (3) have any biological meaning. The aim of this step is to define a set of sufficiently accurate and smooth exchange flux constraints that also address the solution infeasibility issue, hindering the estimation of continuous intracellular flux predictions in dynamic constraint-based models. Then, the 95% confidence interval of transport fluxes were imposed as inequality constraints on  $\mathbf{v}_{Transport}$  vector in equation (2). The generated ranges of intracellular fluxes estimated by DFVA were treated as unbiased bounds with regard to any possibly assumed objective function for the LP problems solved in DFBA (section 6). Of importance, it is a methodologically distinct use of FVA technique in CBM approaches than what the authors followed in (Mahadevan and Schilling, 2003). In their work, the LP problem was first optimized, for example, to maximize the growth rate and then the FVA technique was used to determine the range of the possible alternate optima. The *ad-hoc* metabolic network developed here supports the generation of dynamic unbiased intracellular flux ranges as

Table 2. The Euclidean distance between the DFBA solution sets.

	Set 1	Set 2	Set 3	Set 4
Set 1	0	13737	1591.8	13874
Set 2	13737	0	15308	787.52
Set 3	1591.8	15308	0	15446
Set 4	13874	787.52	15446	0

described in section 5 on a personal computer with Intel(r) Core(TM) i5-8250U CPU @ 1.60 GHz and 8 GB RAM memory. However, a similar analysis on the genome-wide metabolic model of erythrocytes demands significantly higher computation power emphasizing the importance of metabolic modelling integration with state-of-the-art computing techniques (see (Kitano, 2002)).

### 7.3 Multiple alternative objective functions and analysis of the Euclidean distance between dynamic flux distribution optima

In section 6, we solved the DFBA problem for multiple alternative objective functions, but within the same equality and inequality constraints. Then, we used Quadratic Programming (QP) to calculate the Euclidean distance between the four sets of dynamic flux distribution optima as shown in equation (9),

$$\begin{aligned} \text{dist}(\text{set}_i, \text{set}_j) &= \\ &\left( \sum_{k=1}^L \sum_{r=1}^n \left( v_{i,k,r} - v_{j,k,r} \right)^2 \right)^{\frac{1}{2}} \end{aligned} \quad (9)$$

$i, j = 1, 2, 3, 4$

In fact, we intend to show that systemic generation of multiple relevant biological objective functions followed by model-driven analysis of the generated flux distribution optima provides a robust computational approach to systems-level scrutiny of a metabolic network of interest. Thus, in table 2, we reported the symmetrical matrix of dynamic flux distributions Euclidean distance. The results revealed that Set 2 and Set 4 are the closest dynamic flux distribution optima.

### 7.4 Mitigating the solution space infeasibility issue

We know that the biosystem acquires a mass balanced carbon flux distribution at any point within the experimental scope. Therefore, we expect the model to find feasible solutions within the same *in-silico* conditions. Thus, we argue that if the LP optimization solver cannot find a feasible solution in the enzymatic flux vector space  $\mathbb{R}^n$ , then, there exist some limitations in the model (e.g., unfilled gaps, inaccurate mechanistic assumptions, inconsistent model scope, etc), and/or the data are not accurate. We showed that the connectedness of the developed metabolic network and the smoothness of the simulated exometabolomics play important roles in tackling the infeasibility issue regularly associated with stoichiometric-based models (Meadows et al., 2010; Nolan and Lee, 2012). Herein, we managed to generate feasible time-resolved solutions for the fully constrained system by including sink reactions only for a small fraction of the intracellular metabolites, i.e., 14%.

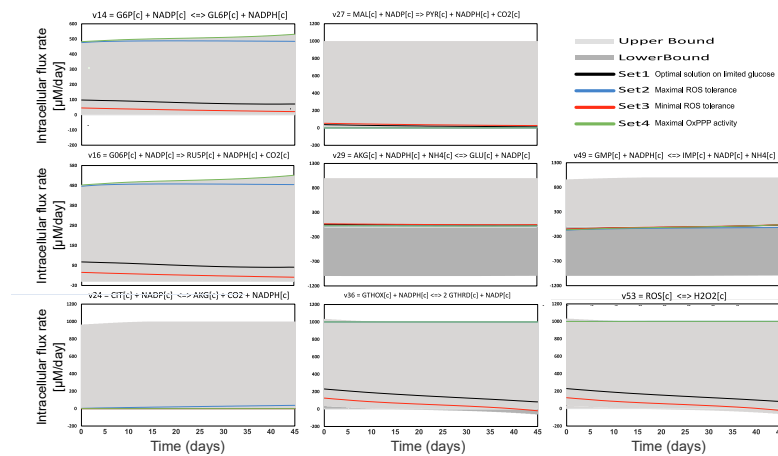


Fig. 2. The dynamics of ROS detoxification and NADPH-dependent reaction rates constrained by dynamic intracellular flux bounds. The colour-coded curves represent optimal flux dynamics associated with the solution set of the four objectives (section 6) and the grey-shaded background represents the dynamic intracellular flux ranges. Set 2 (maximal ROS tolerance in solid blue) and Set 4 (maximal PPP activity in solid green) overlap in v27, v29, v36, and v53.

### 7.5 Using the validated model for generating systems-level biological hypotheses

The results reported in table 2 is in agreement with previous findings supporting the positive correlation between PPP activity and antioxidant defence mechanisms in other biological systems (Moon et al., 2020; Christodoulou et al., 2018). In fact, the oxidative PPP to hexokinase turnover ratio could increase from 106% to 197% in the PPP hyperactivity scenario (set 4). This range was from 21% at day zero to 32% at day 42 of the storage time in the glucose limited nominal scenario (set 1). The carbon flux through the oxidative branch of PPP with 2 moles NADPH turnover for each mole of glucose intake represents a metabolic route to generate reducing cofactors (NADPH), i.e., v14, v15, and v16. We show that the termination of higher fluxes of ROS modelled via v53 to preserve redox homeostasis is possible through a sustained activation of this pathway. We also found that hyper activation of the PPP pathway can pull v2 in its reverse direction and also suppress citrate to alpha-ketoglutarate and malate to pyruvate reactions, possibly because the latter ones are competing for NAD substrates. Such *in-silico* analysis results may suggest a rationale for increasing citrate concentrations in blood bags to compete for the storage lesions consumption through an alternative metabolic route. We also envisage that the same *in-silico* approach could be helpful to characterize the influence of urate on RBC metabolism during storage. Indeed, we showed that the RBC preparation triggers a progressive loss of urate during the first week of storage (Bardyn et al., 2017a). The compensation of this leak by adding urate and ascorbic acid was suspected to reroute the metabolism (switch between oxPPP and glycolysis) (Bardyn et al., 2020). Collectively, these simulation results emphasize the inherent variability in dynamics of cell metabolism and the possible implications of this heterogeneity for the regulation of antioxidant defence machinery.

## 8. CONCLUSION

We have set up a constraint-based model of RBC metabolic network for the mechanistic estimation of the biochemical reaction network fluxes under twelve narrow transport reaction constraints evolving with storage time. The model complemented with different hypotheses can predict flux rates of antioxidant defence systems. We demonstrated that the model generates time-resolved predictions of non-measured fluxes variation with media change, which is essential for systems-based amelioration of the storage lesions (Bardyn et al., 2018, 2020). Finally, we used the model to calculate the distance between the four distinct optimal flux distribution solutions (Fig. 2). Two considerable shortcomings of the presented dynamic metabolic flux methodology are, first, not providing intracellular metabolite levels at this stage, and also, the lack of explicit integration of the metabolic regulation events. Addressing these limitations will be covered in a further modelling study.

## ACKNOWLEDGEMENTS

The authors wish to acknowledge Natural Sciences and Engineering Research Council (NSERC) funding for this project (M.J.).

## REFERENCES

- Bardyn, M., Chen, J., Dussiot, M., Crettaz, D., Schmid, L., Langst, E., Amireault, P., Tissot, J.D., Jolicœur, M., and Prudent, M. (2020). Restoration of physiological levels of uric acid and ascorbic acid reroutes the metabolism of stored red blood cells. *Metabolites*, 10(6). doi:10.3390/metabo10060226.
- Bardyn, M., Maye, S., Lesch, A., Delobel, J., Tissot, J.D., Cortes-Salazar, F., Tacchini, P., Lion, N., Girault, H.H., and Prudent, M. (2017a). The antioxidant capacity of erythrocyte concentrates is increased during the first week of storage and correlated with the uric acid level. *Vox Sang*, 112(7), 638–647. doi:10.1111/vox.12563.

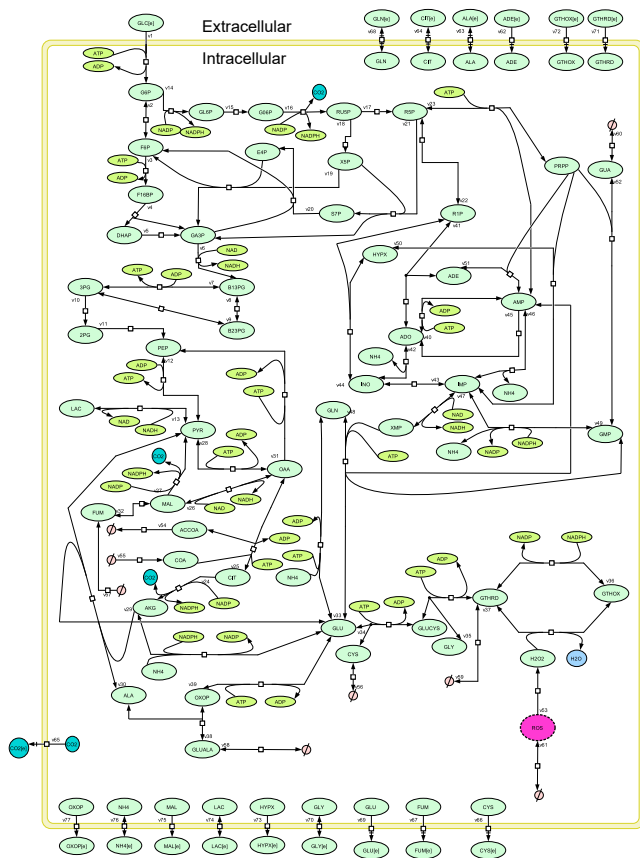


Fig. 3. **The ad-hoc RBC metabolic map** The metabolic network can be divided into ten bioreaction subsystems including, glycolysis (v1-v13), pentose phosphate pathway (v14-v23), TCA cycle (v24-v32), glutamate and glutathione metabolism (v33-v39), purine catabolism (v40-v45), Nucleotides (v46-v49), Salvage pathway (v50-v52), ROS detoxification (v53), sink and demand reactions (v54-v61), and transport reactions (v62-v77).

- Bardyn, M., Rappaz, B., Jaferzadeh, K., Crettaz, D., Tissot, J.D., Moon, I., Turcatti, G., Lion, N., and Prudent, M. (2017b). Red blood cells ageing markers: a multi-parametric analysis. *Blood Transfus*, 15(3), 239–248. doi:10.2450/2017.0318-16.
- Bardyn, M., Tissot, J.D., and Prudent, M. (2018). Oxidative stress and antioxidant defenses during blood processing and storage of erythrocyte concentrates. *Transfus Clin Biol*, 25(1), 96–100. doi:10.1016/j.tracli.2017.08.001.
- Bordbar, A., Jamshidi, N., and Palsson, B.O. (2011). iab-rbc-283: A proteomically derived knowledge-base of erythrocyte metabolism that can be used to simulate its physiological and patho-physiological states. *BMC Syst Biol*, 5(1), 110. doi:10.1186/1752-0509-5-110.
- Bordbar, A., Johansson, P.I., Paglia, G., Harrison, S.J., Wichuk, K., Magnusdottir, M., Valgeirsdottir, S., Gybel-Brask, M., Ostrowski, S.R., Palsson, S., Rolfsson, O., Sigurjonsson, O.E., Hansen, M.B., Gudmundsson, S., and Palsson, B.O. (2016). Identified metabolic signature for assessing red blood cell unit quality is associated with endothelial damage markers and clinical outcomes.

- Transfusion*, 56(4), 852–62. doi:10.1111/trf.13460.
- Christodoulou, D., Link, H., Fuhrer, T., Kochanowski, K., Gerosa, L., and Sauer, U. (2018). Reserve flux capacity in the pentose phosphate pathway enables escherichia coli's rapid response to oxidative stress. *Cell Syst*, 6(5), 569–578 e7. doi:10.1016/j.cels.2018.04.009.
- Kitano, H. (2002). Computational systems biology. *Nature*, 420(6912), 206–10. doi:10.1038/nature01254.
- Lafilaquiere, B., Leclercq, G., Choey, C., Chen, J., Peres, S., Ito, C., and Jolicoeur, M. (2018). Identifying biomarkers of wharton's jelly mesenchymal stromal cells using a dynamic metabolic model: The cell passage effect. *Metabolites*, 8(1). doi:10.3390/metabo8010018.
- Lakrisenko, P. and Weindl, D. (2021). Dynamic models for metabolomics data integration. *Current Opinion in Systems Biology*, 28, 100358. doi:10.1016/j.coisb.2021.100358.
- Mahadevan, R. and Schilling, C.H. (2003). The effects of alternate optimal solutions in constraint-based genome-scale metabolic models. *Metab Eng*, 5(4), 264–76. doi:10.1016/j.ymben.2003.09.002. URL <https://www.ncbi.nlm.nih.gov/pubmed/14642354>.
- Meadows, A.L., Karnik, R., Lam, H., Forestell, S., and Snedecor, B. (2010). Application of dynamic flux balance analysis to an industrial escherichia coli fermentation. *Metabolic engineering*, 12(2), 150–160.
- Moon, S.J., Dong, W., Stephanopoulos, G.N., and Sikes, H.D. (2020). Oxidative pentose phosphate pathway and glucose anaplerosis support maintenance of mitochondrial nadph pool under mitochondrial oxidative stress. *Bioeng Transl Med*, 5(3), e10184. doi:10.1002/btm2.10184.
- Nolan, R.P. and Lee, K. (2012). Dynamic model for cho cell engineering. *J Biotechnol*, 158(1-2), 24–33. doi:10.1016/j.jbiotec.2012.01.009.
- Paglia, G., D'Alessandro, A., Rolfsson, O., Sigurjonsson, O.E., Bordbar, A., Palsson, S., Nemkov, T., Hansen, K.C., Gudmundsson, S., and Palsson, B.O. (2016). Biomarkers defining the metabolic age of red blood cells during cold storage. *Blood*, 128(13), e43–50. doi:10.1182/blood-2016-06-721688.
- Roback, J.D., Josephson, C.D., Waller, E.K., Newman, J.L., Karatela, S., Uppal, K., Jones, D.P., Zimring, J.C., and Dumont, L.J. (2014). Metabolomics of adsol (as-1) red blood cell storage. *Transfus Med Rev*, 28(2), 41–55. doi:10.1016/j.tmr.2014.01.003.
- Segel, L.A. and Slemrod, M. (1989). The quasi-steady-state assumption: A case study in perturbation. *SIAM Review*, 31(3), 446–477. doi:10.1137/1031091.
- Volkova, S., Matos, M.R.A., Mattanovich, M., and Marin de Mas, I. (2020). Metabolic modelling as a framework for metabolomics data integration and analysis. *Metabolites*, 10(8). doi:10.3390/metabo10080303.
- Yasemi, M. and Jolicoeur, M. (2021). Modelling cell metabolism: A review on constraint-based steady-state and kinetic approaches. *Processes*, 9(2). doi:10.3390/pr9020322.
- Yoshida, T., Prudent, M., and D'Alessandro, A. (2019). Red blood cell storage lesion: causes and potential clinical consequences. *Blood transfusion = Trasfusione del sangue*, 17(1), 27–52. doi:10.2450/2019.0217-18.